CS 555 Project:
Adaptivity in Finite Element Methods

Anurag Bhattacharyya
bhttchr6@illinois.edu

1 Problem description

The main problem investigated in this project is the 2d plane stress elasticity problem for a L-shaped domain. Some other numerical experiments have also been explored in the *Appendix* section. The poisson's equation for this elasticity problem is given by

$$\begin{aligned} \nabla^2 u &= -F_b \quad \text{on} \quad \Omega \\ u &= 0 \quad \text{on} \quad \Gamma_d \end{aligned} \tag{1}$$

Here $u = u(x, y)$ is the displacement at the nodes and F_b is the body force acting on the structure. Γ_d represents the fixed boundaries at the top where the prescribed displacements are zero. The domain with the loading and boundary conditions are shown in Figure 1a

Experimental goals:

In this elasticity problem, there is also a body force acting on the entire structure in the downward direction. From elasticity studies we know that the region connecting the overhanging portion to the top fixed boundary will be highly stressed and as a result the error in these elements will be high as well. I expect that the adaptive mesh refinement process will capture these regions of high internal stresses, consequently more error prone, and the mesh will be refined in this region to lower the peak in the internal stress values and subsequenly a reduction in the error norm.

Implementation

The adaptive refinement algorithm follows a cycle of
solve→*estimate*→*mark*→*refine*.
We first start with *solve*. A structural finite element solver was fully developed in-house coupled with the *MeshPy* grid generator. Linear triangular elements was used for meshing the design domain having 2 degrees of freedom at each vertex. A body force to simulate loading due to gravity was impelmented. The undeformed mesh (blue) and the deformed mesh (green) is shown in Figure 1b. After calculating the required values on the initial mesh, we estimate the errors in the elements. For this we use a posteriori error estimator as described in section 2.

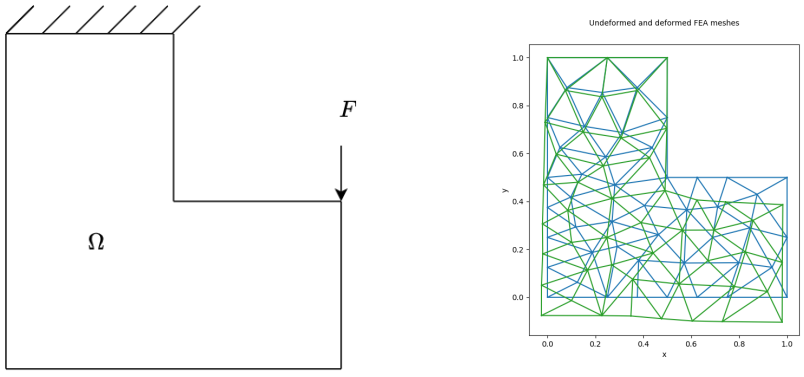

(a) (b)

Figure 1: Design domain and FEA meshes

2 A posteriori error estimator

Error estimators that are based directly on the finite element approximation and data of the problem are usually refered to as *explicit* error estimators. They require less computational effort but they involve compromises in accuracy and robustness.

Explicit error estimators involve a direct computation of the interior element residuals and the jumps at the element boundaries to find an estimate for error. After analysing different expressions for the error estimates, we can write the general form of it as given in [1] and [2] as:

$$||e_h||^2 \leq \sum_{i=0}^{m} \left[c_1 \int_{\Omega_i} ||R||_{L^2}^2 d\Omega + c_2 \int_{I_i} ||J||_{L^2}^2 dI \right] \tag{2}$$

Here, m is the number of elements used to discretize the domain. Terms R is the interior element residual and J is the jump of the gradient across the element edge. I_i is the element interface. The constants c_1 and c_2 are specific to the problem. For our case, following along the lines of [2], we have taken them to be:

$$c_1 = \frac{h^2}{24K}, \quad c_2 = \frac{h}{24K} \tag{3}$$

Here h is the longest edge of the element and $K = \frac{E}{1-\mu}$ for plane stress elasticity problems with linear shape functions. Referring to [1], we can define the rest of the terms in Equation 2 as :

$$R = f + \nabla^2 u_h, \quad J = \boldsymbol{n} \cdot \nabla u_h \tag{4}$$

This result follows from [1]. The general bilinear form can be written as

$$a(u_h, v_h) = l(v_h) \tag{5}$$

For all test functions v_h. The error of the finite element approximation is denoted by $e_h = u - u_h$ and satisfies the error representation

$$a(e_h, v) = l(v) - a(u_h, v) \tag{6}$$

Using summation over the whole domain, we can write

$$a(e_h, v) = \sum_{i=1}^{m} \int_{\omega_i} Rv\dot{\Omega} + \int_{I_i} JvdI \tag{7}$$

Using Galerkin orthogonality condition to for interpolant functions, element-wise Cauchy-Schwartz inequlity and the results of interpolation theory, specifically

$$||v - I_h v||_{L^2} \leq ch||v||_{H^1}, \quad ||v - I_h v|| \leq c\sqrt{h}||v||_{H^1} \tag{8}$$

we can write Equation 2 as the posteriori error estimator equation. The Equation 2 directly leads to a local error indicator n_i defiend by:

$$||e_h||^2 \leq (E_h)^2 = \sum_{i=1}^{m} \eta_i^2 \tag{9}$$

Adaptive procedure and tolerances
The error indicator defined in Equation 9 is used for driving mesh adaptivity. Given the estimate E_h for the error in the energy norm, the relative error is calculated as

$$e_{rel} = \frac{||e_h||}{||u_h||} \approx \frac{E_h}{||u_h||_{L^2}} \tag{10}$$

The strategy used here is to enrich the finite element space, if the relative error e_{rel} exceeds a specific tolerance. For our case, we have used the tolerance value as 0.1. We *mark* the elements with errors exceeding this tolerance value and subsequently *refine* them using *MeshPy*.

2.1 Reliability and efficiency estimates

The reliability and efficiency estimates determine the quality of a posteriori error estimator. They are basically measured by the upper and lower bounds of the error estimator. The *reliability* measure ensures that the error in the elements of the mesh is always less than a positive constant, ensuring that the overall error in the solution is always bounded. The *efficiency* measures quantifies that the estimator does not over-refine the mesh and thereby keeps the computation costs low while achieving a solution.
The error is generally bounded as shown below

$$\gamma\eta \leq ||e|| \leq \Gamma\eta \quad 0 < \gamma \leq \Gamma \tag{11}$$

From Equation (5), we see that it has a upper bound, hence the posteriori error estimate is *reliable*.

3 Re-entrant corner problem

Observations
This original mesh has 96 d.o.f. The stress distribution over the domain is shown in Figure 2. As expected we can observe that the internal stress values are indeed high in the connector region, connecting the hanging part to the fixed regions.

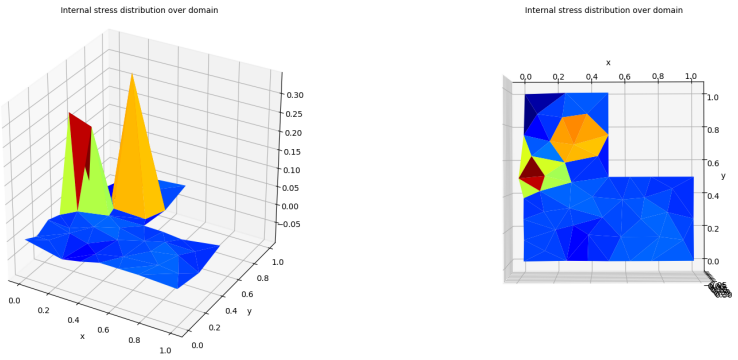

(a) (b)

Figure 2: Internal stress distribution over the initial domain

After applying the adaptive meshing techniques using the error estimator as shown in Equation 2, we get the refined mesh as shown in Figure 3. The refined mesh has 508 degrees of freedom. We do observe that as expected the mesh to be refined in the connector region. The error estimator identifies the elements with high errors and subsequently refines them. The stress distribution over the domain is shown in Figure 4. The L_∞ norm of the internal stress decreased from 0.34533 to 0.1145.

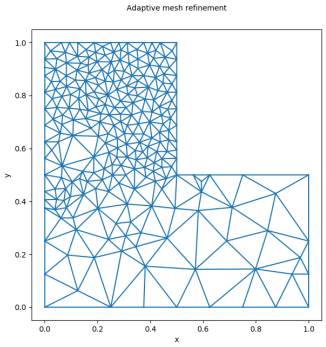

Figure 3: Refined mesh obtained through adaptive refinement techniques

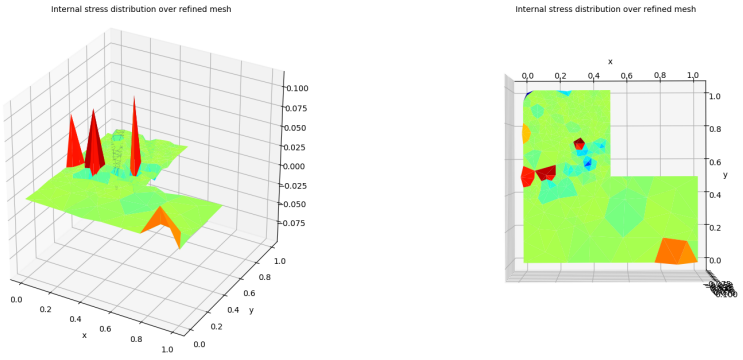

(a) (b)

Figure 4: Internal stress distribution over the adaptively refined domain

Discussion/Concern

I also expected to observe the mesh refinement to be more curved near the re-entrant corner. This is something that is also typically observed in L-domain problems. In this study however we do not observe such regions. Which points towards some issues either with the error estimator or with the refinement strategy which requires more investigation.

3.1 Compare adaptive refinement with pre-refinement

I hereby ran 1 cycle of adaptive refinement procedure consisting *estimate*→*mark*→*refine* and compared the gains obtained just with a single cycle with that of pre-refining

the entire domain. We compared the results for the L_∞ norm of the internal-stress (F_{int}).

Table 1: Adaptive mesh refinement performance

d.o.f	$t(s)$	$\|\|Fint\|\|_{L^\infty}$
96	0.02997	0.34533
508	0.15364	0.1145

Table 2: Whole domain pre-refinement performance parameters

d.o.f	$t(s)$	$\|\|Fint\|\|_{L^\infty}$
452	0.13805	0.3198
564	0.15363	0.2338
674	0.16926	0.2139
812	0.2161	0.2149

From Table 1 and Table 2, we can see that adaptive refinement performs much better than pre-refining the entire mesh and using it for FEM analysis. Even with 812 d.o.f, the L_∞ norm for a uniformly meshed domain is around 46% higher than the one with 508 d.o.f. This strategy

4 Domain with cusps

For domains with cusps the problem rises from the fact that many of the results on Sobolev spaces, which are fundamental for finite element analysis, do not apply because the domain is non-Lipschitz. One way to solve this issue would be to replace the cusped domain with a polygonal domain and use the standard FEM. But numerical examples show that it is sub-optimal to extend the solution obtained through smooth polygonal approximation to domains with cusps. It has been shown that one solution is to use graded meshes in a weighted H^2 space, the weight being a power of the distance to the cuspidal point [3].

5 Critique: Adaptive Mesh Refinement (AMR)

One of the disadvantages of AMR is that a priori convergence is not guaranteed automatically and depends on the algorithmic details. It is not theoretically justified from the start that the AMR will generate an accurate solution at all. Also, the meshes generated in each cycle of AMR are not related to one another which may pose challenges in many cases.

6 Instructions for running the codes

There are two major codes uploaded *FEM_AMR_L_dom.py* and *AMR_FEM_square.py*. Other results were generated using code snippets made from these codes

1. Run *FEM_AMR_L_dom.py*. It will generate 4 figures. Figure window 1 corresponds to Figure 1b at page 2 and Figure window 0 corresponds to Figure 3 at page 5 respectively. Figure window 2 and 4 are the Figure(2) and Figure(4) on pages 4 and 5 respectively.

2. Run *AMR_FEM_square.py*. It will generate 4 figures appropriately titled. Figure window 1 and 2 correspond to Figure (5) and Figure (8) at pages 8 and 10 respectively. Figure window 3 and 4 correspond to Figure (6) at page 8.

References

[1] T. Grätsch and K.-J. Bathe, "A posteriori error estimation techniques in practical finite element analysis," *Computers & structures*, vol. 83, no. 4-5, pp. 235–265, 2005.

[2] O. C. Zienkiewicz and J. Z. Zhu, "A simple error estimator and adaptive procedure for practical engineerng analysis," *International journal for numerical methods in engineering*, vol. 24, no. 2, pp. 337–357, 1987.

[3] G. Acosta, M. G. Armentano, R. G. Durán, and A. L. Lombardi, "Finite element approximations in a nonlipschitz domain," *SIAM journal on numerical analysis*, vol. 45, no. 1, pp. 277–295, 2007.

A Appendix

A.1 Some more experimental studies

Let us also analyze a toy Poisson's problem with known solution to characterise FEM performance. Let us start with the Equation 12 :

$$\begin{aligned} \nabla^2 u &= -2\pi^2 \sin(\pi x)\sin(\pi y) \quad \text{on} \quad \Omega \\ u &= 0 \quad \text{on} \quad \partial\Omega \end{aligned} \tag{12}$$

This equation was chosen because of the existence of its exact solution as shown in Equation (2), which could guide us regarding solution checking while implementing the adaptive FEM procedure.

$$u = \sin(\pi x)\cos(\pi y) \tag{13}$$

We will first take a look at a smooth boundary domain and then move on to a domain with re-entrant corner.

A.2 Square domain

We solve Equation 12 on a square domain.

$$\begin{aligned} \nabla^2 u &= -2\pi^2 \sin(\pi x)\sin(\pi y) \quad \text{on} \quad \Omega \in [-1,1]\times[-1,1] \\ u &= 0 \quad \text{on} \quad \partial\Omega \end{aligned} \tag{14}$$

The initial mesh on this domain is shown below:

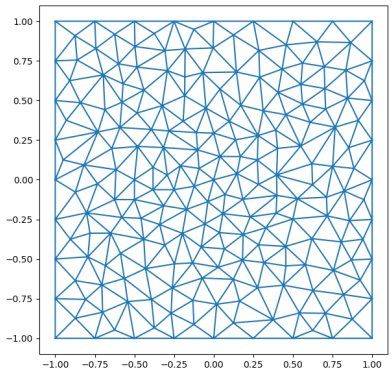

Figure 5: Initial design domain with mesh

A mesh with 207 degrees of freedom is created as shown in Figure (5) and is used to obtain the FEM solution. The FEM solution and the exact solutions are shown below

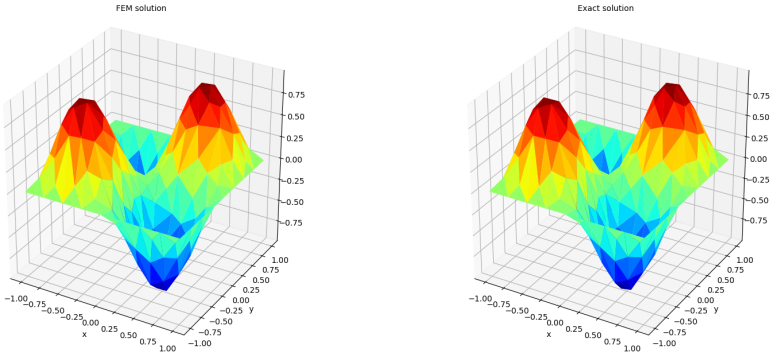

(a) FEM solution (b) Exact solution

Figure 6: Comparison of FEM solution and exact solution

Let us see what information can be extracted with the exact and true solutions for the case with smooth boundaries. Since we also have the exact solution, we can carry out some analysis regarding error estimators. Let us start with priori error estimates.

A.3 A priori error estimates

This states that if u_h is a piecewise linear finite element approximation to the exact solution u on a mesh with maximum element size h. Then

$$||u - u_h||_{L_2} \leq Ch^2||u''||_{L_2} \tag{15}$$

Table 3 shows the relation between the element size(h), the l.h.s and the r.h.s of Equation 15.

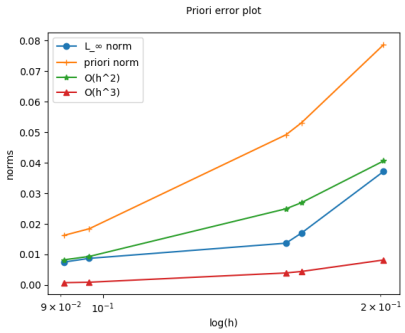

Figure 7: Comparison of error norms

We observe from the Figure 7, that L_∞ error in the piecewise linear method is $\approx O(h^2)$

Table 3: Comparison for priori error norms and element sizes

h	**d.o.f**	$\|\|u - u_h\|\|_{L_2}$	$C\|\|u''\|\|_{L_2}$
0.20154	207	0.13604	0.55345
0.16415	412	0.11508	0.52756
0.15794	609	0.09039	0.60068
0.09665	808	0.075678	0.25911
0.09069	1008	0.06897	0.25646

B A posteriori error estimate results

Using the a posteriori error estimator as defined earlier and using the same marking and refinement procedure, from the original mesh shown in Figure 5,

we obtain the adaptively refined mesh as shown in Figure 8. The L_2 norm on the nodal solution vector values shows a decrease from 0.1360 for the original mesh to 0.1165 for the adaptively refined mesh.

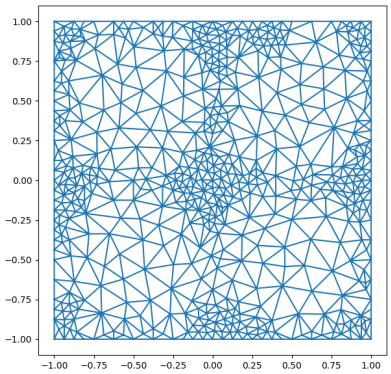

Figure 8: Adaptive mesh refinement on square domain

Solving Equation 12 with the same boundary conditions on a L-shaped domain using FEM gives us a solution as shown in Figure 9. Applying adaptive refinement procedure gives us the results as shown in Figure 10. The L_2 norm reduces from 0.12468 for the original mesh to 0.9825 for the refined mesh.

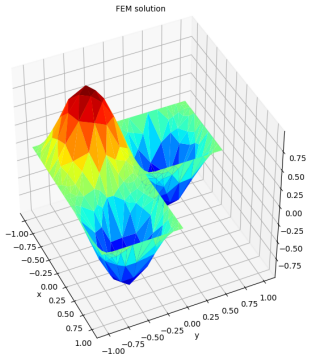

Figure 9: FEM solution on L-domain

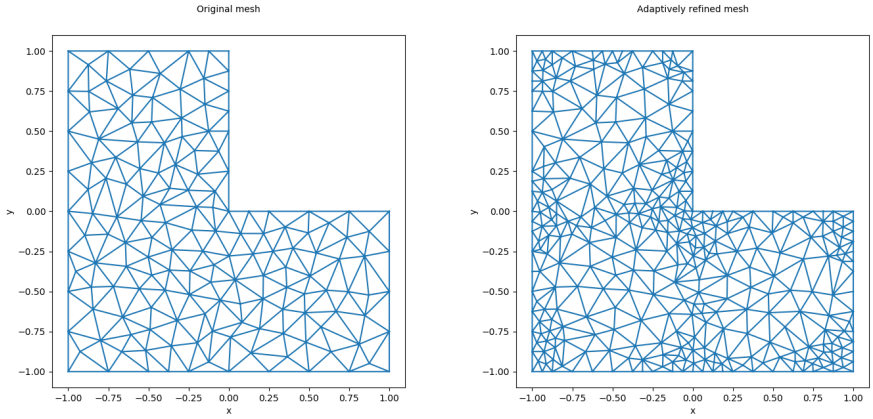

(a) original mesh (b) adaptively refined mesh

Figure 10: Adaptive refinement on L-shaped domain

Observations If we compare the locations where the mesh gets adaptively refined with the FEM solution for the L-shaped and the square domain, we observe that the mesh is primarily refined in the regions either along the boundaries or in the regions where there is a superimposition of results with large changes in magnitudes (like if we see the mesh refinement at the centre of the domain for the square mesh in Figure 8). This is because in these regions errors are higher due to boundaries and superposition.